Position-sensitive change in the transition metal L-edge fine structures

Ahmet Gulec, Patrick J. Phillips, and Robert F. Klie

Citation: Applied Physics Letters **107**, 143111 (2015); doi: 10.1063/1.4932637
View online: http://dx.doi.org/10.1063/1.4932637
View Table of Contents: http://scitation.aip.org/content/aip/journal/apl/107/14?ver=pdfcov
Published by the AIP Publishing

Position-sensitive change in the transition metal *L*-edge fine structures

Ahmet Gulec, Patrick J. Phillips, and Robert F. Klie
Department of Physics, University of Illinois at Chicago, Chicago, Illinois 60607, USA

(Received 13 July 2015; accepted 26 September 2015; published online 8 October 2015)

Studying the structure and composition of solid-state materials on the atomic scale has become nearly routine in transmission electron microscopy with the development of novel electron optics and electron sources. In particular, with spatial resolutions better than 0.1 nm and energy resolution smaller than 100 meV, the stoichiometry, bonding, and coordination can now be examined on similar scales. Aberration-corrected scanning transmission electron microscopy and electron energy-loss spectroscopy (EELS) have played a crucial role in identifying charge ordering, valence, and as spin state transitions in transition metal perovskite oxides. In this letter, we investigate the effects of ever-decreasing electron-probe sizes on the measured near-edge fine-structure of the transition metal core-loss edge using EELS. We find that for certain transition metal perovskites, the position of the electron probe with respect to the atomic column is crucial in determining the correct valence state. Several reasons for the observed position-sensitive EELS fine-structure are discussed. © *2015 AIP Publishing LLC*. [http://dx.doi.org/10.1063/1.4932637]

Over the last two decades, the scanning transmission electron microscope (STEM) in combination with electron energy-loss spectroscopy (EELS) has become increasingly more popular for quantifying the local electronic structure and composition of materials. EELS measures the energy loss in an electron beam as a result of inelastic scattering from interactions with a sample. For core-level excitations, as discussed in this Letter, closely bound inner shell electrons are excited into unoccupied chemical orbitals. While the first atomic-column resolved EELS measurements were reported in 1993,[1–3] the spatial resolution was limited by the electron probe size of 2 Å and the low electron dose rates. Moreover, spectra were taken manually from each atomic column to minimize sample drift.[1–4] However, with the incorporation of aberration correctors into scanning transmission electron microscopes in the late 1990s, the electron probe sizes have decreased dramatically, now reaching better than 50 pm spatial resolution in the latest generation of aberration-corrected STEM/TEMs.[5–10] With that improvement in spatial resolution also comes a significant increase in the available probe currents, which now enables the acquisition of entire hyper-spectral images (or spectrum images) with atomic resolution.[11,12]

In addition to measuring the local composition, EELS also allows for the determination of the local density of states, bonding, as well as the local valence or spin state.[13] In transition metal oxides, especially in perovskite oxides, EELS has been used to measure the valence state of virtually every transition metal element.[13–15] Starting with $SrTiO_3$, atomic-resolution EELS has been proven to be a powerful technique to determine the Ti valence state by recording the Ti L_3/L_2 core-loss edges as a function of position across grain boundaries[4] and hetero-interfaces.[16] The spatial resolution of such measurements was primarily determined by the electron probe size, assuming the inter-column separation is larger than the probe size and an appropriately large collection angle for the EEL spectrometer is chosen.[17]

Atomic-column resolved EELS has been employed to measure a wide array of properties, including the charge ordering in manganites, the accumulation of charges at grain boundaries and dislocation cores in several perovskite oxides, as well as the effects of oxygen vacancy ordering.[18,19] All these valence state determinations rely on measuring the transition metal *L*-edges and comparing the fine-structure, more specifically the L_3/L_2-ratio, to known standards. Several different methods have been developed to extract the L_3/L_2-ratios, including the second derivative approach, which appears to be the most reliable.[20] In addition, the edge onset of the transition metal *L*-edges and the O *K*-edge fine structures have been used to quantify the transition metal valence states, but to a lesser extent.[21] Recently, EELS has also been used to determine the spin-state of transition metals, such as Co^{3+}, using either the Co *L*-edges or the O *K*-edges.[22–24] All these analyses can now be conducted with single atomic-column sensitivity and resolution.

In this Letter, we demonstrate that for certain perovskite oxides, such as $(Pr_{0.85},Y_{0.15})_{0.7}Ca_{0.3}CoO_3$, $BiFeO_3$, and Sr-doped $LaCoO_3$, the quantification of the transition metal oxide valence state is not as straight forward as previously suggested, if the electron probe size is significantly smaller than the interatomic distances in that projection. We will demonstrate that the transition metal *L*-edge fine-structure shows a strong dependence on the exact position of the electron probe with respect to the atomic column. We will compare this effect with that in samples that do not show this position sensitivity, such as $La_{0.8}Sr_{0.2}MnO_3$, $SrTiO_3$ or $BaTiO_3$, and attempt to explain these effects based on the residual probe-aberrations and initial states of the excited atomic columns.

The spectrum images shown in this Letter were acquired using the JEOL JEM-ARM200CF at UIC, a probe aberration-corrected STEM/TEM equipped with a 200 kV cold-field emission gun, a post-column Gatan Enfina EEL spectrometer and a variety of annular dark and bright field detectors.[8] While the JEOL JEM-ARM200CF at UIC can achieve a spatial resolution better than 70 pm at 200 kV,[8] for this work, the electron probe size was chosen to be 1 Å with a probe current of 62 pA during the EELS using a

convergence angle of 25 mrad and an EELS collection angle of 75 mrad. The elemental maps shown here are generated using a standard procedure. More specifically, the exponential background was fitted over an energy range of 50 eV prior to the respective edge onset and then subtracted from the core-loss spectrum. The signal for each element is integrated over a 20 eV energy window and the plotted as a function of position. The white-line or L_3/L_2 ratios for the different transition metal L-edges are calculated using the second derivative method as integrated in the Gatan Microscopy Suite (GMS2.3) using parameters previously reported in Ref. 20.

The initial EELS analysis focuses on several cobalt-oxide materials, such as $(Pr_{0.85},Y_{0.15})_{0.7}Ca_{0.3}CoO_3$ and Sr-doped $LaCoO_3$. Each sample was analyzed in either the pseudo-cubic [110] or [001] orientation, and EEL spectrum images were acquired across several unit-cells in the respective orientation with at least 5 pixels per atomic column. Figure 1 shows an example of $(Pr_{0.85},Y_{0.15})_{0.7}Ca_{0.3}CoO_3$ in the pseudo-cubic [001] orientation where the oxygen, cobalt, and praseodymium sublattices can be clearly identified. The calcium sublattice was also imaged, but is not shown here. Next, we analyze the Co L-edges in an attempt to determine the Co valence state. The calculated Co L_3/L_2-ratio map is shown in Figure 1(b) and the extracted EEL spectrum of the Co L- and Pr M-edges is shown in Figure 1(c). As indicated in Figure 1(b), the calculated Co L_3/L_2-ratio varied between 2.72 and 3.01 (with a standard deviation of ± 0.05) as a function of electron probe position with respect to the Co atomic columns. When the electron probe is located on top of a Co atomic column, the Co L_3/L_2-ratio appears to be 3, corresponding to a Co valence of 3.3+. However, between the Co atomic columns the L_3/L_2-ratio decreases significantly, indicating an apparent increase in the Co valence state closer to 4+.

A similar effect is observed in Sr-doped $LaCoO_3$ materials over a range of Sr-doping concentrations (see Figures 2, 3 and 4(a)). In all four Co-based perovskite oxides, the measured Co valence state, as determined by the Co L_3/L_2-ratio, appears to depend significantly on the electron probe position and varies from the expected Co valence state to a significantly higher valence state when measured between two Co columns.

This effect of position-sensitive changes in the near-edge fine structure was previously reported for the O K-edge, where it was shown to depend on the electron probe position within the crystal structure unit cell.[25] In Figures 3(d) and 3(e), we show the relative O K-edge pre-peak intensity as a function of position for the case of $La_{0.83}Sr_{0.17}CoO_3$. It can be clearly seen that the relative O K-edge pre-peak intensity is highest when the electron probe is on the oxygen atomic columns and lowest when the probe is on the Co atomic columns. The position sensitivity of the O K-edge can be understood by considering the origin of the O K-edge pre-peak intensity. Stemming from transitions of the O 1s core-level states, the O K-edge pre-peak measures the density of unoccupied states into the hybridized Co 3d-O 1s orbitals. Since the majority of electron momentum transfer occurs in the direction perpendicular to the incoming electron beam,[26–28] the orientation of the final states is as important as the position of the impinging electron probe. For example, if the electron beam probes the pure oxygen columns in $La_{0.83}Sr_{0.17}CoO_3$ [001] the higher O K-edge pre-peak intensity is due to the high density of hybridized Co-

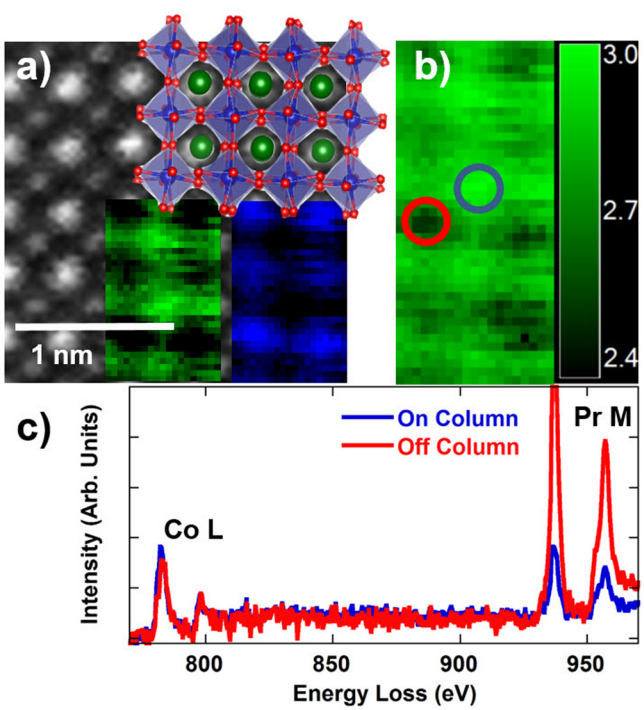

FIG. 1. (a) Atomic-resolution high-angle annular dark field (HAADF) image of $(Pr_{0.85},Y_{0.15})_{0.7}Ca_{0.3}CoO_3$ in the pseudo-cubic [001] orientation. A model of the $(Pr_{0.85},Y_{0.15})_{0.7}Ca_{0.3}CoO_3$ structure, as well as the EEL spectrum images of the Co L- and Pr M- edges are shown as insets in green and blue, respectively. (b) Map of the Co L_3/L_2-ratio and (c) EEL spectra from locations indicated in (b) showing the changes in fine-structure depending on the probe location.

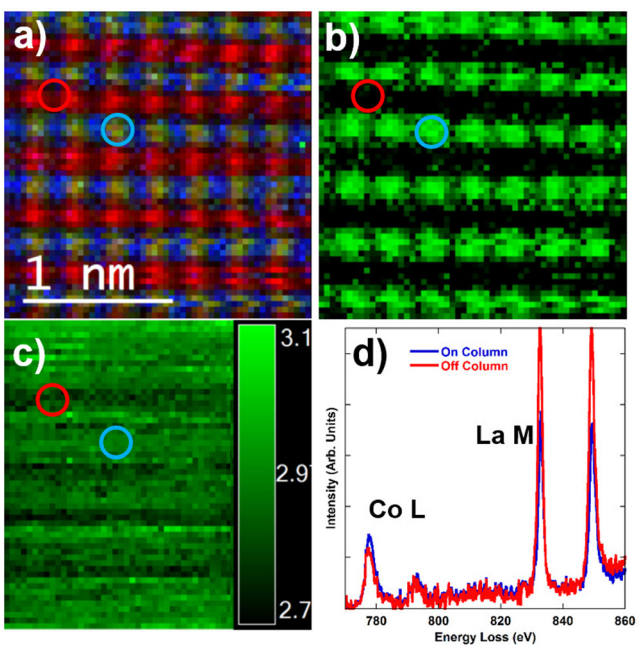

FIG. 2. (a) Atomic-column resolved EELS map of $La_{0.7}Sr_{0.3}CoO_3$ in the pseudo cubic [011] orientation with the La/Sr columns shown in red, Co in blue and oxygen in green. (b) EEL spectrum image of the integrated Co L-edge intensity. (c) EELS map of the Co L_3/L_2-ratio. A comparison of Co L- and La M-edges taken from red and blue circles is shown in (d).

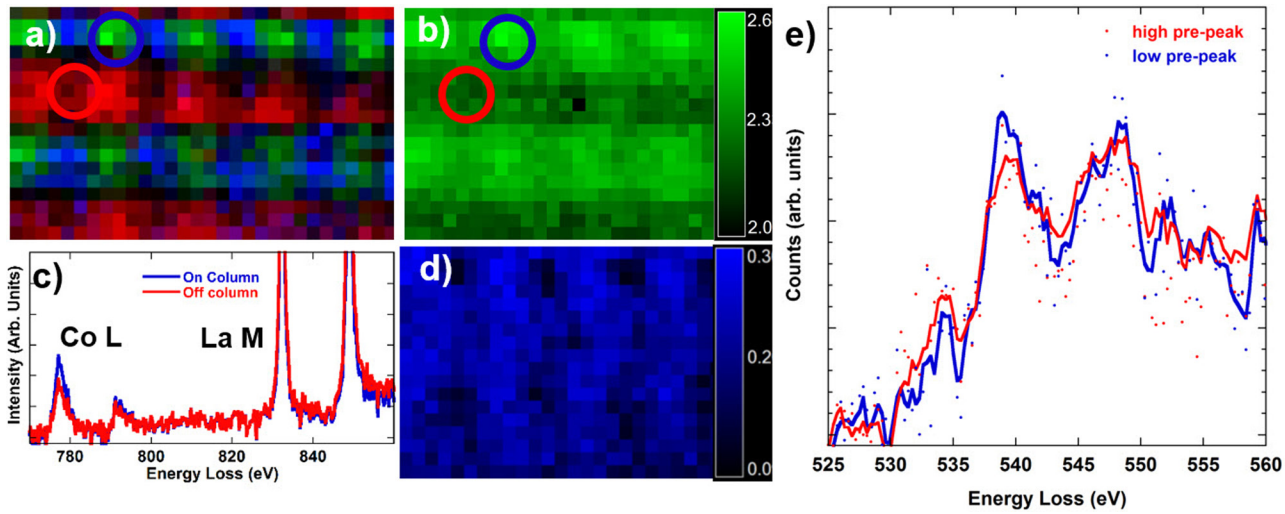

FIG. 3. (a) Atomic-column resolved EELS map of $La_{0.83}Sr_{0.17}CoO_3$ in the pseudo cubic [011] orientation with the La/Sr columns shown in red, Co in blue, and oxygen in green. (b) EELS map of the Co L_3/L_2-ratio. A comparison of Co L- and La M-edges taken from red and blue circles is shown in (d). (d) The relative O K-edge pre-peak intensity map normalized by total O K-edge intensity. (e) O K-edge spectra extracted from (d) showing high and low pre-peak intensities. The solid lines are smoothed by 0.6 eV, and the dots show the raw data.

O orbitals in the plane perpendicular to the incoming beam. On the other hand, on the Co atomic columns, the hybridized Co-O orbitals, as measured by the O K-edge are only parallel to the electron beam and the pre-peak intensity is therefore significantly lower. This nearly universal effect on the O K-edge, however, appears to be fundamentally different from the changes in the transition metal L-edges described earlier, since the orientation of the transition-metal orbitals does not affect the L_3/L_2 ratios.

Figure 4(b) shows two atomic-column resolved EEL spectra of $BiFeO_3$. The Fe L-edges as a function of position on or off the Fe atomic columns show again significant fluctuations, indicating an apparent change in the local Fe valence state. Using previously acquired reference samples, and assuming that the Fe is in the 3+ oxidation state, the apparent decrease in the Fe L_3/L_2-ratio would correspond to a decrease in the Fe valence state to ≈2+.

For $La_{0.8}Sr_{0.2}MnO_3$, $BaTiO_3$, as well as $SrTiO_3$, none of the effects described for the previous transition metal L_3/L_2-ratios are observed. Figure 5 shows the atomic-column resolved EEL spectra for $La_{0.8}Sr_{0.2}MnO_3$, $BaTiO_3$, and $SrTiO_3$, respectively. As can be clearly seen in Figure 5, the transition metal L-edge fine structure remains unchanged regardless of the electron-probe position. This effect is particularly clear in $SrTiO_3$ (Figure 5(c)), where the Ti L-edges show the expected crystal field splitting due to the Ti^{4+} $3d$ t_{2g} and e_g final states. However, the crystal field splitting is present in all the Ti L edge spectra, regardless of the electron probe position. This observed crystal-field splitting of the L edges is due to the Ti $3d^0$ occupancy, and is absent in spectra of Ti^{3+}.[29] $BaTiO_3$ also shows the fine-structure for Ti^{4+}, and the Ti L-edge fine-structure remains unchanged as the electron probe moves (Figure 5(b)). A similar insensitivity to the electron probe position is observed for the Mn L-edges in $La_{0.8}Sr_{0.2}MnO_3$ (Figure 5(a)).

There are several possible explanations for this observed effect which we will discuss next. The energy onset of the transition-metal L-edge increases from ≈460 eV for the titanates to ≈770 eV for the cobaltates. Concomitant with this increase in edge onset is also a decrease in the near-edge fine-structure, as the t_{2g} orbitals are being populated and the crystal field splitting is no longer present or resolvable using the given energy resolution of the cold-field emission source (350 meV). The position sensitivity of the transition metal L-edge is only observed for Co and Fe containing oxides, where the transition-metal edge onset is higher than ≈710 eV and the fine-structure of the L-edge is not resolved. To rule out the effect of noise on the reported results we have taken numerous spectrum images and point spectra with increasing acquisition times, and reproducibly find the same position sensitivity reported above. The explanation of a spectrum imaging analysis artifact can, therefore, be ruled out.

While both Ti and Mn are early transition metals with less than half-filled $3d$ orbitals, Fe and Co have $4s^2\,3d^6$ and $4s^2\,3d^7$ occupancy, respectively. One possible explanation

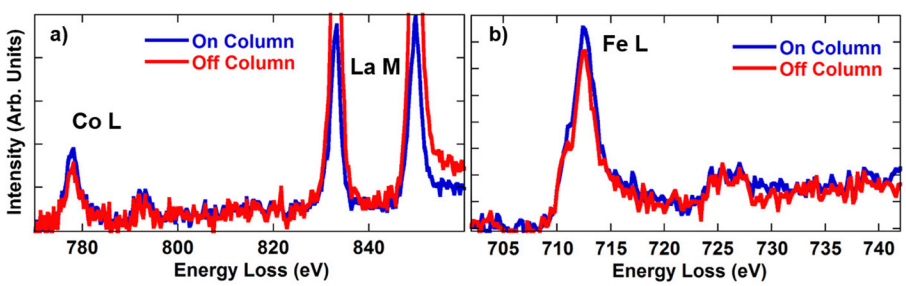

FIG. 4. EELS spectra of the (a) Co L- and La M-edges in $La_{0.95}Sr_{0.05}CoO_3$ and (b) the Fe L-edges in $BiFeO_3$.

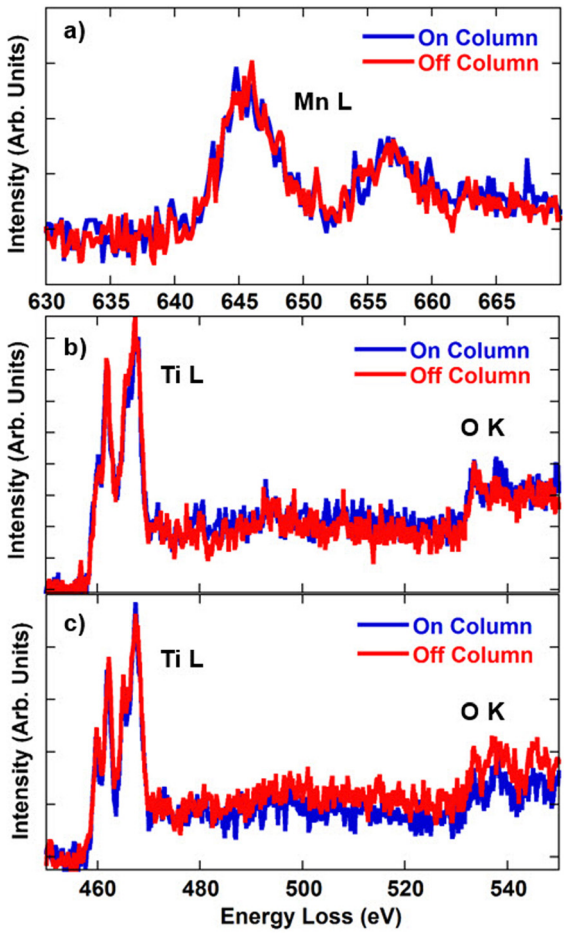

FIG. 5. Atomic-column resolved EEL spectra of (a) the Mn *L*-edges in $La_{0.8}Sr_{0.2}MnO_3$, and the Ti *L*- and O *K*-edges in (b) $BaTiO_3$ and (c) $SrTiO_3$. The transition metal *L*-edges does not exhibit any changes as a function of position.

for the position sensitivity is the dependence on the 3*d* orbital occupancy and the related spatial extent of the available final states. However, the 3*d* orbital occupancy of transition-metal oxides is different from that of simple transition metals. In both $SrTiO_3$ and $BaTiO_3$, the valence state of Ti is 4+, which means that the Ti 3*d* orbitals are completely empty. For $LaMnO_3$, the Mn^{3+} 3*d* orbitals exhibit a $t_{2g}^3 e_g^1$ configuration with a local spin of the localized t_{2g} electrons of $S = 3/2$. At increasing hole concentration, $LaMnO_3$ turns into a ferro-magnetic metal due to the delocalization of the charge carriers via the double exchange interaction between the Mn^{3+} and Mn^{4+} site. Both the t_{2g} and e_g orbitals are (partially) occupied, leaving both orbitals open to transitions from the initial Mn 2*s* orbitals. However, we did not find any position sensitivity for the Mn *L*-edges in $La_{0.8}Sr_{0.2}MnO_3$. On the other hand, $LaCoO_3$, the parent compound for $La_{0.7}Sr_{0.3}CoO_3$, $La_{0.83}Sr_{0.17}CoO_3$ and $La_{0.95}Sr_{0.05}CoO_3$, is known to undergo several spin-state transitions at 80 K and above 450 K. For increasing Sr-doping, the spin state increases with the presence of Co^{4+}, which reduces the e_g occupancy. Similar orbital occupancy has been reported for $(Pr_{0.85},Y_{0.15})_{0.7}Ca_{0.3}CoO_3$. However, despite the less than half-filled 3*d* orbital, the structures containing Co show a strong dependence of the *L*-edge fine structure on the electron probe position. Finally, $BiFeO_3$ has a spin state of 5/2, with partially filled t_{2g} and e_g orbital, and exhibits strong position dependence. So, it appears that neither the 3*d* orbital occupancy nor the spin-state of the transition metal correlates with the observed position dependence of the transition metal L_3/L_2-ratio.

Rusz and coworkers have reported that atomic resolution dichroism measurements are possible without using an electron vortex beam carrying orbital angular momentum.[30] Interestingly, Rusz *et al.* also discuss the effects of the electron probe position on the dichroic signal in magnetically ordered systems and conclude that the change in the transition metal L_3/L_2-ratio due to the presence of magnetic ordering is decreased as *x*, the distance from the atomic column, increases.[30] While this can explain the lack of position sensitivity for $SrTiO_3$ and $BaTiO_3$, the position sensitivity for $(Pr_{0.85},Y_{0.15})_{0.7}Ca_{0.3}CoO_3$ and the Sr-doped $LaCoO_3$ samples do not fit the magnetic dichroism picture.

The role of increasing 4*s* character of the final states on the position sensitivity of the L_3/L_2-ratio and the effects of the initial transition metal 2*p* states on the position dependence need also be considered. Finally, the fact that this effect was not previously observed in EELS measurements conducted in conventional TEM mode or STEM, neither in X-ray absorption spectroscopies, indicates that the residual higher order aberrations, or the highly localized electron probe, are responsible for the position sensitive *L*-edge fine structure for certain perovskite oxides described above. The highly focussed electron beam in the aberration-corrected STEM provides a probe with much higher localization. The observed position dependence of the transition metal *L*-edges just represents the change of the electron wave-function distribution along the transition metal-oxide columns. For higher 3*d* transition metals, the 3*d* states are highly localized, so the distribution gradient is stronger, while for lower 3*d* transition metals, like Mn^{2+}, the 3*d* states are much less localized. For now, this effect might just be very weak for lower transition metals and but could be visualized with better signal-to-noise-ratio spectra. For Ti^{4+}, where the 3*d* orbital are empty, there will be no effect as a function of probe position. Careful modeling of the transition metal near-edge fine-structure and evaluations of the mixed dynamic form factor are necessary to explain these effects.

The authors thank J. F. Mitchell and C. Leighton for providing the samples and for the stimulating discussions. This work was supported by a grant from the National Science Foundation (Grant No. DMR-1408427). The acquisition of the UIC JEOL JEM-ARM200CF was supported by a NSF MRI-R^2 Grant (DMR-0959470). Support from the UIC Research Resources Center (RRC), in particular, A.W. Nicholls is acknowledged.

[1]N. D. Browning, M. F. Chrisholm, and S. J. Pennycook, Nature **366**, 143 (1993).
[2]D. A. Muller, Y. Tzou, R. Raj, and J. Silcox, Nature **366**, 725 (1993).
[3]P. E. Batson, Nature **366**, 727 (1993).
[4]R. F. Klie and N. D. Browning, Appl. Phys. Lett. **77**, 3737 (2000).
[5]P. E. Batson, N. Dellby, and O. L. Krivanek, Nature **418**, 617 (2002).
[6]O. L. Krivanek, P. D. Nellist, N. Dellby, M. F. Murfitt, and Z. Szilagyi, Ultramicroscopy **96**, 229 (2003).

[7]O. L. Krivanek, M. F. Chisholm, V. Nicolosi, T. J. Pennycook, G. J. Corbin, N. Dellby, M. F. Murfitt, C. S. Own, Z. S. Szilagyi, M. P. Oxley, S. T. Pantelides, and S. J. Pennycook, Nature **464**, 571 (2010).
[8]R. F. Klie, A. Gulec, Z. Guo, T. Paulauskas, Q. Qiao, R. Tao, C. Wang, K. B. Low, A. W. Nicholls, and P. J. Phillips, Cryst. Res. Technol. **49**, 653 (2014).
[9]R. F. Klie, J. P. Buban, M. Varela, A. Franceschetti, C. Jooss, Y. Zhu, N. D. Browning, S. T. Pantelides, and S. J. Pennycook, Nature **435**, 475 (2005).
[10]P. D. Nellist, M. F. Chisholm, N. Dellby, O. L. Krivanek, M. F. Murfitt, Z. S. Szilagyi, A. R. Lupini, A. Borisevich, W. H. Sides, Jr., and S. J. Pennycook, Science **305**, 1741 (2004).
[11]D. A. Muller, L. F. Kourkoutis, M. Murfitt, J. H. Song, H. Y. Hwang, J. Silcox, N. Dellby, and O. L. Krivanek, Science **319**, 1073 (2008).
[12]P. J. Phillips, T. Paulauskas, N. Rowlands, A. W. Nicholls, K.-B. Low, S. Bhadare, and R. F. Klie, Microsc. Microanal. **20**, 1046 (2014).
[13]R. F. Egerton, *Electron Energy Loss Spectroscopy in the Electron Microscope* (Plenum Press, New York, 1986).
[14]Z. L. Wang, J. Bentley, and N. D. Evans, Micron **31**, 355 (2000).
[15]L. F. Kourkoutis, H. Xin, T. Higuchi, Y. Hotta, J. Lee, Y. Hikita, D. Schlom, H. Hwang, and D. Muller, Philos. Mag. **90**, 4731 (2010).
[16]Q. Qiao, R. F. Klie, S. Ogut, and J. C. Idrobo, Phys. Rev. B **85**, 165406 (2012).
[17]E. Cosgriff, M. Oxley, L. Allen, and S. Pennycook, Ultramicroscopy **102**, 317 (2005).
[18]M. Varela, A. R. Lupini, K. van Benthem, A. Y. Borisevich, M. F. Chisholm, N. Shibata, E. Abe, and S. J. Pennycook, Annu. Rev. Mater. Res. **35**, 539 (2005).
[19]N. Biskup, J. Salafranca, V. Mehta, M. P. Oxley, Y. Suzuki, S. J. Pennycook, S. T. Pantelides, and M. Varela, Phys. Rev. Lett. **112**, 087202 (2014).
[20]S. Stemmer, A. Sane, N. D. Browning, and T. J. Mazanec, Solid State Ionics **130**, 71 (2000).
[21]M. Sankararaman and D. Perry, J. Mater. Sci. **27**, 2731 (1992).
[22]R. F. Klie, J. C. Zheng, Y. Zhu, M. Varela, J. Wu, and C. Leighton, Phys. Rev. Lett. **99**, 047203 (2007).
[23]J.-H. Kwon, W. S. Choi, Y.-K. Kwon, R. Jung, J.-M. Zuo, H. N. Lee, and M. Kim, Chem. Mater. **26**, 2496 (2014).
[24]R. F. Klie, Q. Qiao, T. Paulauskas, A. Gulec, A. Rebola, S. Ogut, M. P. Prange, J. C. Idrobo, S. T. Pantelides, S. Kolesnik, B. Dabrowski, M. Ozdemir, C. Boyraz, D. Mazumdar, and A. Gupta, Phys. Rev. Lett. **108**, 196601 (2012).
[25]R. F. Klie, Q. Qiao, T. Paulauskas, Q. Ramasse, M. P. Oxley, and J. C. Idrobo, Phys. Rev. B **85**, 054106 (2012).
[26]R. F. Klie, H. Su, Y. Zhu, J. W. Davenport, J. C. Idrobo, N. D. Browning, and P. D. Nellist, Phys. Rev. B **67**, 144508 (2003).
[27]N. D. Browning, J. Yuan, and L. M. Brown, Ultramicroscopy **38**, 291 (1991).
[28]N. D. Browning, J. Yuan, and L. M. Brown, Philos. Mag. A **67**, 261 (1993).
[29]A. Ohtomo, D. A. Muller, J. L. Grazul, and H. Y. Hwang, Nature **419**, 378 (2002).
[30]J. Rusz, J.-C. Idrobo, and S. Bhowmick, Phys. Rev. Lett. **113**, 145501 (2014).